Supplemental Material for "Probing ground-state phase transitions through quench dynamics"

Paraj Titum, Joseph T. Iosue, James R. Garrison, Alexey V. Gorshkov, and Zhe-Xuan Gong

In this Supplemental Material, we provide details of calculations referenced in the main text. Section S.I focuses on analytical results of the nearest-neighbor transverse-field Ising model (TFIM), deriving Eqs. (4) and (6) and Fig. 2 of the main text and discussing the finite-size and finite-time scaling properties of the derivative of the nearest-neighbor correlator. In Sec. S.II, we provide details of the self-consistent mean-field calculations, which were used in the main text to estimate the location of the critical point in the TFIM with next-nearest-neighbor interactions. In Sec. S.III, we remark briefly on the scaling properties in the presence of integrability breaking to explain the scaling collapse in Fig. 3 of the main text. In Sec. S.IV, we describe the numerical method we used for time evolution. Finally, in Sec. S.V, we show that the dynamical critical point analyzed in Sec. S.I exists for a wide class of initial states.

S.I. ANALYTICAL CALCULATION DETAILS FOR NEAREST-NEIGHBOR TFIM

In this section, we provide details for the analytical results of the nearest-neighbor transverse field Ising model. In Secs. S.I A and S.I B, we review the well known method of diagonalizing the Hamiltonian and representing the initial state. In Sec. S.I C, we calculate the analytical formula for the time dependence of the nearest-neighbor correlator, $G(t)$. Finally, in Sec. S.I D, we compare the finite-time and finite-size scaling of the derivative, $\frac{\partial G_{\text{av}}(t)}{\partial B}$.

A. Diagonalizing the Hamiltonian

The Jordan-Wigner transformation from spins to free fermions is defined as follows:

$$\sigma_i^x = \left(a_i + a_i^\dagger\right) e^{i\pi \sum_{j<i} a_j^\dagger a_j}, \tag{S1}$$

$$\sigma_i^y = i\left(a_i - a_i^\dagger\right) e^{i\pi \sum_{j<i} a_j^\dagger a_j}, \tag{S2}$$

$$\sigma_i^z = 2a_i^\dagger a_i - 1. \tag{S3}$$

Under the Jordan-Wigner transformation, the nearest-neighbor transverse-field Ising model with periodic boundary conditions [Eq. (1) with $\Delta = 0$] transforms to a free fermion model,

$$H_\eta = J\sum_{i=1}^{L-1}\left(a_i - a_i^\dagger\right)\left(a_{i+1} + a_{i+1}^\dagger\right) + B\sum_{i=1}^{L}(2a_i^\dagger a_i - 1) + \eta\left(a_L - a_L^\dagger\right)\left(a_1 + a_1^\dagger\right). \tag{S4}$$

Here, $\eta = \exp\left(i\pi\sum_j a_j^\dagger a_j\right)$ is the parity of the fermion number, with $\eta = 1$ for an even number of fermions and $\eta = -1$ for an odd number of fermions. We can now take advantage of the translation symmetry in H_η by using a Fourier transformation, $b_{q_\eta} = \frac{1}{\sqrt{L}}\sum_{j=1}^{L} a_j e^{iq_\eta j}$ where $q_\eta = \frac{\pi}{L}\left[2m + \frac{1}{2}(\eta - 1)\right]$ with $m \in \left\{-\frac{L}{2}+1, \cdots 0, 1, \cdots, \frac{L}{2}\right\}$. This gives us

$$H_\eta = 2J\sum_{q_\eta>0} \mathbf{b}^\dagger \begin{pmatrix} \frac{B}{J} - \cos q_\eta & i\sin q_\eta \\ -i\sin q_\eta & -\frac{B}{J} + \cos q_\eta \end{pmatrix} \mathbf{b}, \tag{S5}$$

with $\mathbf{b} = \begin{pmatrix} b_{q_\eta} & b_{-q_\eta}^\dagger \end{pmatrix}^T$. This can now be diagonalized using a Bogoliubov transformation, $\gamma_{q_\eta} = u_{q_\eta} b_{q_\eta} + i v_{q_\eta} b_{-q_\eta}^\dagger$, with $u_{q_\eta} = \cos\theta_{q_\eta}$, $v_{q_\eta} = \sin\theta_{q_\eta}$, and $\tan 2\theta_{q_\eta} = \frac{J\sin q_\eta}{B - J\cos q_\eta}$. In this basis we obtain the diagonal Hamiltonian

$$H_\eta = \sum_{q_\eta>0} \omega_{q_\eta}\left(\gamma_{q_\eta}^\dagger\gamma_{q_\eta} + \gamma_{-q_\eta}^\dagger\gamma_{-q_\eta} - 1\right), \tag{S6}$$

with $\omega_{q_\eta} = 2J\sqrt{\frac{B^2}{J^2} - 2\frac{B}{J}\cos q_\eta + 1}$. The ground state is $|\phi_0\rangle \equiv \frac{1}{|v_{q_\eta}|}\prod_{q_\eta>0}\gamma_{q_\eta}\gamma_{-q_\eta}|0\rangle$, where $|0\rangle \equiv |\downarrow\cdots\downarrow\rangle$ is the vacuum state of the a_i operators. All excited states can be written down as a set of excitations with momenta denoted by $\{Q_\eta\}$:

$$|\phi_n\rangle = \prod_{q_\eta\in\{Q_\eta\}} \gamma_{q_\eta}^\dagger|\phi_0\rangle = \prod_{q_\eta} |p_{n,q_\eta} p_{n,-q_\eta}\rangle, \tag{S7}$$

where $p_{n,q_\eta} = \langle\phi_n|\hat{I}_{q_\eta}|\phi_n\rangle = 0$ or 1, denoting the occupation of the mode with momentum q_η.

B. Initial state and expectation values

We choose the initial state to have all spins polarized along the x direction:

$$|\psi_{\text{in}}\rangle = |{\to_x}\cdots{\to_x}\rangle = \frac{1}{2^{L/2}}\left(1 + a_1^\dagger\right)\cdots\left(1 + a_L^\dagger\right)|0\rangle. \tag{S8}$$

Note that the initial state $|\psi_{\rm in}\rangle$ is a superposition of both even ($\eta=1$) and odd ($\eta=-1$) parity sectors. We can write the initial state as an equal-weighted superposition of both parity sectors, $|\psi_{\rm in}\rangle = \frac{1}{\sqrt{2}}\left(|\psi_{\rm in}^{\eta=1}\rangle + |\psi_{\rm in}^{\eta=-1}\rangle\right)$. We provide analytical expressions for the expectation values of various operators in this initial state projected to a given parity sector:

$$\left\langle b_{q_\eta}^\dagger b_{q_\eta}\right\rangle_{{\rm in},\eta} = \frac{1}{2L}\left[L+(L-2)\cos q_\eta\right], \tag{S9}$$

$$\left\langle b_{-q_\eta} b_{-q_\eta}^\dagger\right\rangle_{{\rm in},\eta} = \frac{1}{2L}\left[L-(L-2)\cos q_\eta\right], \tag{S10}$$

$$\left\langle b_{q_\eta}^\dagger b_{-q_\eta}^\dagger\right\rangle_{{\rm in},\eta} = \frac{i\,(L-2)}{2L}\sin q_\eta, \tag{S11}$$

$$\left\langle b_{-q_\eta} b_{q_\eta}\right\rangle_{{\rm in},\eta} = -\frac{i\,(L-2)}{2L}\sin q_\eta, \tag{S12}$$

$$\left\langle \gamma_{q_\eta}^\dagger \gamma_{q_\eta}\right\rangle_{{\rm in},\eta} = \frac{1}{2L}\left[L-2\,(L-2)\,\frac{J-B\cos q_\eta}{\omega_{q_\eta}}\right], \tag{S13}$$

$$\left\langle \gamma_{q_\eta}\gamma_{q_\eta}\right\rangle_{{\rm in},\eta} = -\frac{i\,(L-2)\sin q_\eta}{L\omega_{q_\eta}}B, \tag{S14}$$

where $\langle\cdots\rangle_{{\rm in},\eta} = \langle\psi_{\rm in}^\eta|\cdots|\psi_{\rm in}^\eta\rangle$, and $|\psi_{\rm in}^\eta\rangle$ is assumed to be normalized.

C. Time dependence of $G(t)$

In this section, we obtain the time dependence of the correlator analytically. The nearest-neighbor correlator was defined in Eq. (3) in the main text. Using the Jordan-Wigner transformation, we obtain an expression for the operator that measures the nearest-neighbor correlator,

$$\begin{aligned}\hat{G}_\eta = &-\frac{1}{L}\sum_{q_\eta>0}(-2\cos q_\eta)\left(b_{q_\eta}^\dagger b_{q_\eta} - b_{-q_\eta}b_{-q_\eta}^\dagger\right)\\ &+2i\sin q_\eta\left(b_{q_\eta}b_{-q_\eta}+b_{q_\eta}^\dagger b_{-q_\eta}^\dagger\right).\end{aligned} \tag{S15}$$

Note that this expression depends upon the fermion number parity η through the definition of q_η. The correlation operator $\hat{G}_\eta$ does not change the parity of the state it acts on. Therefore the expectation value of the time-dependent correlator can be written as

$$G(t) = \frac{1}{2}\left[\langle\psi_{\rm in}^{\eta=1}|\hat{G}_1(t)|\psi_{\rm in}^{\eta=1}\rangle + \langle\psi_{\rm in}^{\eta=-1}|\hat{G}_{-1}(t)|\psi_{\rm in}^{\eta=-1}\rangle\right]. \tag{S16}$$

Recall from the previous section that the expectation values of the conserved densities, I_{q_η}, in the initial state are only dependent on the parity through q_η, just like in Eq. (S15). Therefore, the analytical expression for the contribution from both sectors will be the same and we can drop the dependence on η in q_η in all expressions and evaluate the formula of $G(t)$ using Eqs. (S9) to (S14). Going to the Bogoliubov basis, we can exactly calculate the time dependence,

$$\hat{G}(t) = \hat{G}_0 + \frac{1}{L}\sum_{q>0}\frac{4B\sin q}{\omega_q}i\left(\gamma_{-q}\gamma_q e^{-2i\omega_q t} + \text{H.c.}\right), \tag{S17}$$

where the q sum is taken over values allowed for either parity, and where

$$\hat{G}_0 = \sum_q \frac{1-2\gamma_q^\dagger\gamma_q}{\omega_q}\left[-2\cos q\,(B-J\cos q)+2J\sin^2 q\right]. \tag{S18}$$

Taking an expectation value with respect to the initial state recovers the analytical expressions for $G_{\rm av}(t)$ and $G^\infty_{\rm av,arbitrary}$ in Eqs. (4) and (6) of the main text. Now, we can obtain an analytical expression for the first derivative of $G_{\rm av}(t)$ with respect to B:

$$\begin{aligned}\frac{\partial G_{\rm av}(t)}{\partial B} = &\frac{(L-2)}{L^2}\sum_q\frac{16B\sin^2 q}{\omega_q^4}\Big[2J\,(B\cos q - J)+\\ &+B\,(B-J\cos q)\cos(2t\omega_q)\\ &-\left(B^2+BJ\cos q-2J^2\right)\frac{\sin(2t\omega_q)}{2t\omega_q}\Big].\end{aligned} \tag{S19}$$

In the main text, we use Eq. (S19) to obtain the time dependence of the first derivative in Fig. 2.

D. Scaling of the derivative, $\frac{\partial G_{\rm av}(t)}{\partial B}$

1. *Finite-time scaling*

Let us consider the finite-time scaling of the first derivative of the correlator defined in Eq. (S19). We are interested in the behavior near the critical point. With this in mind, let us consider an expansion around $B = J+\epsilon$. Noting that $\left.\frac{\partial G_{\rm av}(t)}{\partial B}\right|_{B=J} = -\frac{1}{2J}$, we expand around the critical point,

$$\begin{aligned}\left.\frac{\partial G_{\rm av}(t)}{\partial B}\right|_{B=J+\epsilon} \approx &-\frac{1}{2J}\int_0^\pi\frac{dq}{2\pi}\Bigg((1+\cos q)\left[2-\cos(2\omega_q t)-\frac{\sin(2\omega_q t)}{2\omega_q t}\right]\\ &-\frac{\epsilon}{J}\cot^2\left(\frac{q}{2}\right)\left[2+\left(1+\sin^2\left(\frac{q}{2}\right)\right)\cos(2\omega_q t)-\left(64J^2t^2\sin^4\left(\frac{q}{2}\right)+\sin^2\left(\frac{q}{2}\right)+3\right)\frac{\sin(2\omega_q t)}{2\omega_q t}\right]\Bigg),\end{aligned} \tag{S20}$$

where we have used $\omega_q = 2J\sqrt{2(1-\cos q)}$ and taken the thermodynamic limit. Let us examine the above expansion term by term. At $O(\epsilon^0)$, the integrand contains terms $\propto \cos(2\omega_q t)$ and $\frac{\sin(\omega_q t)}{2\omega_q t}$, which average out to zero as time increases. This explains why the derivative is very weakly dependent on time at the critical point ($\epsilon = 0$). Going to the next order at $O(\epsilon)$, we need to be careful around $q \to 0$, since the summand has terms $\propto \frac{1}{\sin^2(q/2)} \sim \frac{1}{q^2}$. Expanding this term around $q = 0$, we obtain the following expression for the derivative near the critical point,

$$\frac{\partial G_{\rm av}(t)}{\partial B} \approx -\frac{1}{2J} + \frac{\epsilon t}{J}\mathcal{F}(Jt), \tag{S21}$$

with

$$\mathcal{F}(x) = \frac{1}{x}\int_0^\pi \frac{dq}{2\pi}\frac{2}{q^2}\left(2+\cos(4xq) - 3\frac{\sin(4xq)}{4xq}\right). \tag{S22}$$

Note that in the limit of large x, $\mathcal{F}(x)$ approaches 1, and we can expand $\frac{\partial G_{\rm av}(t)}{\partial B}$ near $B = J$ as

$$\left.\frac{\partial G_{\rm av}(t)}{\partial B}\right|_{B=J+\epsilon} = \frac{1}{J}\left(-\frac{1}{2} + \epsilon t\right). \tag{S23}$$

This linear dependence is shown as a red dashed line in the inset of Fig. 2 in the main text.

2. *Finite-size scaling*

Now let us discuss the comparison between finite-time scaling and finite-size scaling. In order to isolate the scaling with system size, we examine the infinite-time-averaged value of the first derivative, $\frac{\partial G_{\rm av}(t\to\infty)}{\partial B}$. Utilizing the expression for the derivative expanded around the critical point (but for finite system sizes), we obtain the following expression for the infinite-time-averaged value of the derivative:

$$\begin{aligned}\left.\frac{\partial G_{\rm av}(t\to\infty)}{\partial B}\right|_{B=J+\epsilon} &= -\frac{1}{2J} + \frac{\epsilon}{J^2 L}\sum_{\eta,q_\eta>0}\frac{4}{q_\eta^2} \\ &\approx \frac{1}{J}\left(-\frac{1}{2} + \frac{\epsilon}{3J}L\right).\end{aligned} \tag{S24}$$

Note that for the above expression, the different parity sectors ($\eta = \pm 1$) contribute differently to the coefficient of ϵ. Compared to Eq. (S23), we find that the time t plays the role of $L/(3J)$, where $v = 3J$ can be regarded as a Lieb-Robinson velocity. As a result, the finite-time scaling is in some sense equivalent to the finite-size scaling.

S.II. SELF-CONSISTENT MEAN-FIELD CALCULATIONS FOR TFIM WITH NEXT-NEAREST-NEIGHBOR INTERACTIONS

In this section, we provide details of the self-consistent mean-field calculations we performed to estimate the critical point of the TFIM in the presence of next-nearest-neighbor interactions. In general, this model cannot be mapped to a free-fermion model, and therefore we need to make some approximations to calculate its critical point analytically.

Before doing a self-consistent calculation, let us outline properties of a simpler, noninteracting Hamiltonian,

$$\tilde{H} = J\sum_i \left(a_i - a_i^\dagger\right)\left(a_{i+1} + a_{i+1}^\dagger\right) + J\Delta\sum_i \left(a_i - a_i^\dagger\right)\left(a_{i+2} + a_{i+2}^\dagger\right) + B\sum_{i=1}^{L}\left(2a_i^\dagger a_i - 1\right). \tag{S25}$$

Equation (S25) can be diagonalized in a straightforward manner after Fourier transformation to obtain the quasiparticle spectrum

$$\omega_q = 2J\sqrt{g^2 + 1 + \Delta^2 - 2g(\cos q + \Delta\cos 2q) + 2\Delta\cos q}, \tag{S26}$$

where we have defined $g \equiv B/J$. The quasiparticle annihilation operator is defined analogously as $\gamma_q = \cos\theta_{q_\eta} b_q + i\sin\theta_{q_\eta} b_{-q}^\dagger$, with $\tan 2\theta_{q_\eta} = \frac{\sin q + \Delta\sin 2q}{g - \cos q - \Delta\cos 2q}$ and $b_q = \frac{1}{\sqrt{L}}\sum_j a_j e^{iqj}$. The critical point is at $g = 1 + \Delta$, where it is easy to verify that $\omega_q = 0$ has a solution at $q = 0$. We can now calculate long-time ($t \to \infty$) values of different correlators for dynamics under the Hamiltonian given by Eq. (S25):

$$\mathcal{O}_0 = -\frac{1}{L}\sum_i \left\langle 2a_i^\dagger a_i - 1\right\rangle_{{\rm in},t\to\infty} = \frac{2J}{L}\sum_q \frac{1 - 2\langle I_q\rangle_{\rm in}}{\omega_q}(g - \cos q - \Delta\cos 2q), \tag{S27}$$

$$\mathcal{O}_1 = -\frac{1}{L}\sum_i \left\langle \left(a_i - a_i^\dagger\right)\left(a_{i+1} + a_{i+1}^\dagger\right)\right\rangle_{{\rm in},t\to\infty} = \frac{2J}{L}\sum_q \frac{1 - 2\langle I_q\rangle_{\rm in}}{\omega_q}\left[(\Delta - g)\cos q + 1\right], \tag{S28}$$

$$\mathcal{O}_2 = -\frac{1}{L}\sum_i \left\langle \left(a_i - a_i^\dagger\right)\left(a_{i+2} + a_{i+2}^\dagger\right)\right\rangle_{{\rm in},t\to\infty} = \frac{2J}{L}\sum_q \frac{1 - 2\langle I_q\rangle_{\rm in}}{\omega_q}\left[(\Delta - g\cos 2q + \cos q)\right], \tag{S29}$$

where $\langle\cdots\rangle_{\rm in}$ indicates expectation value with respect to the initial state, and $I_q = \gamma_q^\dagger\gamma_q$ is the quasiparticle density at momentum q. Examining the functional dependence of the correlators, it is clear that starting from the initial state $|\rightarrow\cdots\rightarrow\rangle$, the long-time values of the operators will exhibit a nonanalyticity at the critical point given by $B/J = 1+\Delta$.

Now let us discuss the Ising model with next-nearest-neighbor interactions as defined in Eq. (1). Under the Jordan-Wigner transformation, it becomes

$$H_{\rm NNN} = J\sum_i \left(a_i - a_i^\dagger\right)\left(a_{i+1} + a_{i+1}^\dagger\right) + J\Delta\sum_i \left(a_i - a_i^\dagger\right)\left(1 - 2a_{i+1}^\dagger a_{i+1}\right)\left(a_{i+2} + a_{i+2}^\dagger\right) + B\sum_{i=1}^{L}\left(2a_i^\dagger a_i - 1\right). \quad \text{(S30)}$$

In order to do a self-consistent calculation, we approximate the four-fermion term with a 'Hartree-Fock' like expansion [S1]. While this is standard when considering the ground state of $H_{\rm NNN}$, we extend this approximation to the long-time quench dynamics by taking the mean-field expectation values in the $t\to\infty$ limit with respect to the initial state $|\psi_{\rm in}\rangle$:

$$\begin{aligned}\left(a_i - a_i^\dagger\right)\left(1 - 2a_{i+1}^\dagger a_{i+1}\right)\left(a_{i+2} + a_{i+2}^\dagger\right) \approx{}& \left\langle\left(a_i - a_i^\dagger\right)\left(a_{i+2} + a_{i+2}^\dagger\right)\right\rangle_{{\rm in},t\to\infty}\left(1 - 2a_{i+1}^\dagger a_{i+1}\right)\\ &+ \left\langle\left(1 - 2a_{i+1}^\dagger a_{i+1}\right)\right\rangle_{{\rm in},t\to\infty}\left(a_i - a_i^\dagger\right)\left(a_{i+2} + a_{i+2}^\dagger\right)\\ &- \left\langle\left(a_i - a_i^\dagger\right)\left(a_{i+1} + a_{i+1}^\dagger\right)\right\rangle_{{\rm in},t\to\infty}\left(a_{i+1} - a_{i+1}^\dagger\right)\left(a_{i+2} + a_{i+2}^\dagger\right)\\ &- \left(a_i - a_i^\dagger\right)\left(a_{i+1} + a_{i+1}^\dagger\right)\left\langle\left(a_{i+1} - a_{i+1}^\dagger\right)\left(a_{i+2} + a_{i+2}^\dagger\right)\right\rangle_{{\rm in},t\to\infty},\end{aligned} \quad \text{(S31)}$$

where we drop terms that can be ruled out by the symmetry of the Hamiltonian and the initial state. Plugging this expansion back into the Hamiltonian, we obtain an effective Hamiltonian of the form given by $\tilde{H}$ in Eq. (S25) but with the following the modified parameters:

$$J' = J + 2J\Delta\mathcal{O}_1', \quad \text{(S32)}$$
$$J'\Delta' = J\Delta\mathcal{O}_0', \quad \text{(S33)}$$
$$B' = B + J\Delta\mathcal{O}_2', \quad \text{(S34)}$$

where $\mathcal{O}_i'$ are computed using Eqs. (S27) to (S29) with the replacement $\{J,\Delta,B\}\to\{J',\Delta',B'\}$. The critical point is given by $\Delta' = 1+g'$, which coupled with the above equations gives us the value of the field B at the critical point. In the following, we will discuss two possible cases of solving these self-consistent equations:

1. **Ground state**: For the ground state of Eq. (S30) after the mean-field approximation, we have $\langle I_q\rangle_{\rm gs} = 0$. We obtain the following system of equations for the critical point:

$$J' = J\left(1 + 4\Delta I_1\right), \quad \text{(S35)}$$
$$2J\Delta I_1 = \left(g' - 1\right)\left(J\left(1 + 4\Delta I_1\right) - 2J\Delta I_2\right), \quad \text{(S36)}$$
$$B = g'J' - 2J\Delta\left(g'I_2 - I_1\right), \quad \text{(S37)}$$

with $I_1 = J'\int_{-\pi}^{\pi}\frac{dq}{2\pi}\frac{1}{\omega_q'}\left(-\cos q + 1\right)$ and $I_2 = J'\int_{-\pi}^{\pi}\frac{dq}{2\pi}\frac{1}{\omega_q'}\left(-\cos 2q + 1\right)$, and where ω_q' is given by Eq. (S26) with $\{J,\Delta,B\}\to\{J',\Delta',B'\}$. When Δ is small, these self-consistent equations can be solved analytically to obtain $B\approx J + \frac{16}{3\pi}J\Delta$. For general Δ, these equations can be solved numerically. For instance, at $\Delta = 0.1$, we obtain $B/J = 1.16$ as the critical point.

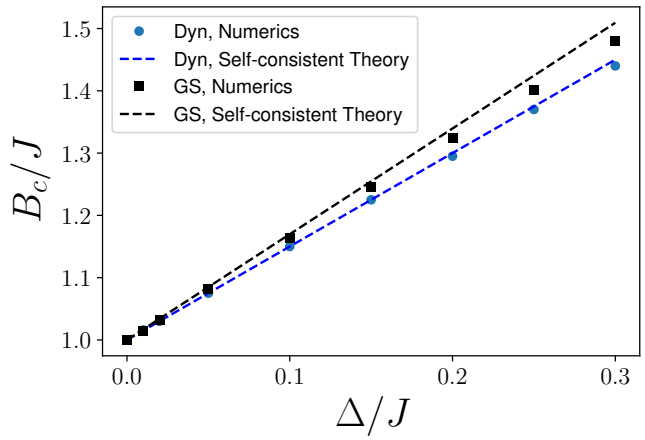

FIG. S1. Comparison between the self-consistent theory and exact numerics. Blue points show the dynamical critical points obtained from finite-time scaling as a function of the integrability breaking. In comparison, the blue dashed line shows the prediction from the mean-field approximation. Black points show the quantum critical point obtained from the finite-size scaling of the Binder cumulant, $\mathcal{U}_4$. The black dashed line shows the expected dependence from the self-consistent mean-field approximation for the ground state.

2. **Quench from** $|\rightarrow\cdots\rightarrow\rangle$: In this case, $\langle I_q\rangle_{\rm in} = \frac{1}{2} - \frac{J'}{\omega_q'}\left[1 - \left(g' - \Delta'\right)\cos q\right]$. Again, the critical point is given by

$$\left(g' - 1\right)\left(g' + \Delta\right) = \Delta\frac{2g' - 1}{2g'}, \quad \text{(S38)}$$
$$B = J\left(g' + \Delta\right). \quad \text{(S39)}$$

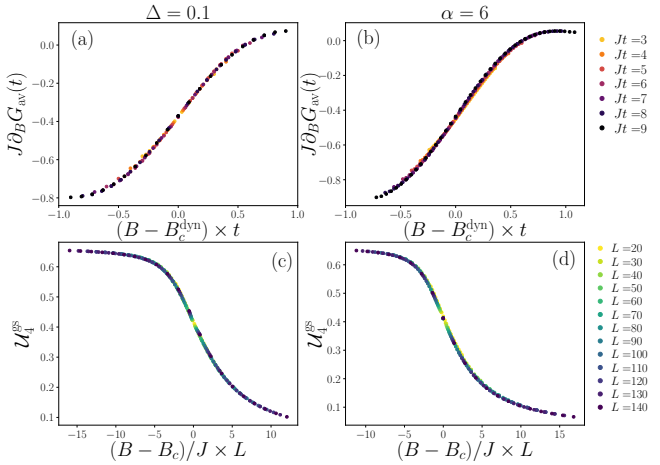

FIG. S2. Scaling collapse with parameters given by the respective panels of Fig. 3 in the main text. The first column [panels (a) and (c)] corresponds to the TFIM with next-nearest-neighbor interaction $\Delta = 0.1$ [Eq. (1)], while the second column [panels (b) and (d)] corresponds to the TFIM with long-range interaction $\alpha = 6$ [Eq. (2)]. The top panels [(a) and (b)] show finite-time scaling of the time-averaged nearest-neighbor correlator $G_{\rm av}(t)$, while the bottom panels [(c) and (d)] show finite-size scaling of the ground-state Binder cumulant $\mathcal{U}_4^{\rm gs}$.

The above equations can be solved to first order in Δ, which gives us the critical point at $B \approx J + \frac{3}{2}J\Delta$.

Note that in general, the self-consistent equations give different solutions for the critical point when using the ground-state or the quench dynamics. In Fig. S1, we compare the predictions for the critical points from the self-consistent theory (both ground-state and quench) with the actual critical points obtained from numerics. We locate the critical points for different values of Δ using the technique employed for Figs. 3(a) and (c) of the main text. Figure S1 shows reasonable agreement between the self-consistent theory and the numerical values.

S.III. SCALING COLLAPSE FOR FIG. 3

In this section, we briefly remark on the scaling properties in the presence of integrability breaking. In Fig. S2, we show the scaling collapse under rescaling of the x axis of Fig. 3. The important thing to note is the distinction between Fig. S2 panels (a) and (b) in comparison with (c) and (d). While the dynamical data collapses to a universal function around the dynamical critical point with $\frac{\partial G_{\rm av}(t)}{\partial B} = \tilde{f}\left((B - B_c^{\rm dy})t\right)$, the ground-state Binder cumulant collapses to a different universal function around the quantum critical point, $\mathcal{U}_4^{\rm gs} = K((B - B_c^{\rm gs})L/J)$.

S.IV. NUMERICAL ALGORITHM FOR TIME EVOLUTION

In this section, we present the numerical method we used for performing time evolution. We assume a spin-half model on N sites in which the Hamiltonian can be decomposed as

$$H = H_x + H_z, \tag{S40}$$

with H_x diagonal in the x basis and H_z diagonal in the z basis. The method takes advantage of the identity $X = \mathsf{H}Z\mathsf{H}$, where $\mathsf{H} = \frac{1}{\sqrt{2}}\begin{pmatrix} 1 & 1 \\ 1 & -1 \end{pmatrix}$ is the Hadamard operator, and X and Z are Pauli matrices. It relies on a fast Walsh-Hadamard transform to apply H to all spins simultaneously. A similar method has been discussed for simulating a kicked Ising model [S2].

Let us first consider the method using a first-order Trotter decomposition,

$$e^{-iH\tau} = e^{-iH_x\tau}e^{-iH_z\tau} + O(\tau^2). \tag{S41}$$

We now consider implementing this operator, which approximates evolution for a time τ, on a state vector $|\psi\rangle$ which is represented in the z basis. The operator $e^{-iH_z\tau}$ can be applied in $O(2^N)$ time since it is diagonal in the z basis. It remains to apply $e^{-iH_x\tau}$. Note that the operator can be written in the form

$$e^{-iH_x\tau} = \mathsf{H}_{\rm all}e^{-iD\tau}\mathsf{H}_{\rm all}, \tag{S42}$$

with $D = \mathsf{H}_{\rm all}H_x\mathsf{H}_{\rm all}$ diagonal in the z basis, and where $\mathsf{H}_{\rm all} = \prod_j \mathsf{H}_j$ is the Hadamard operator applied to all sites j. The operator $\mathsf{H}_{\rm all}$ can be applied to a state in time $O(2^N N)$ and without memory overhead via the fast Walsh-Hadamard transform, which is faster than the equivalent dense matrix multiplication. In this way, the full Trotter time step can be applied by performing two element-wise multiplications of the state vector to implement the diagonal operators, along with two Walsh-Hadamard transforms. The Walsh-Hadamard transform can even be performed in parallel across many cores or nodes in a cluster, e.g. as implemented in FFTW [S3]. If the diagonal elements of H_x and H_z are computed on the fly, the method results in zero memory overhead, unlike Krylov-space methods.

In fact, we can improve the error due to the finite time step by using a fourth-order Suzuki-Trotter decomposition [S4],

$$e^{-iH\tau} = U(\tau_1)U(\tau_1)U(\tau_3)U(\tau_1)U(\tau_1) + O(\tau^5), \tag{S43}$$

where $U(\tau_i) = e^{-iH_z\tau_i/2}e^{-iH_x\tau_i}e^{-iH_z\tau_i/2}$, $\tau_1 = \frac{\tau}{4-4^{1/3}}$, and $\tau_3 = \tau - 4\tau_1$. (Note that τ_3 is actually negative.) The simulations within this paper were obtained by using such a fourth-order decomposition with $\tau = 0.005$. Benchmarking against exact diagonalization suggests that this time step is sufficiently small for the simulations in this paper.

We note that given a maximum permissible error of ϵ (as quantified by the trace distance), the number of Walsh-Hadamard transforms required to simulate for time T is at most $O(T^{5/4}\epsilon^{1/4})$ for such a fourth-order decomposition [S5]. (Here we assume that error from the Suzuki-Trotter decomposition dominates and error from the Walsh-Hadamard transform is negligible.) Recent evidence suggests

that this rigorous error bound may not be tight (see, e.g., Ref. [S6]).

Finally, we note that generalizations of the Walsh-Hadamard transform can be used to implement additional terms in the Hamiltonian, e.g., a term H_y that is diagonal in the y basis.

S.V. MORE GENERAL INITIAL STATES

In this section, we show that the dynamical critical point analyzed in Sec. S.I exists for more general initial states than the product state that is fully polarized in the x direction. We show that the following three types of changes to this initial state do not alter the dynamical critical behavior in any major way: (i) any global rotation of the spins' polarization in the $x-y$ plane, (ii) any small global rotation of the spins' polarization away from the $x-y$ plane, and (iii) any local rotations of the spins. These situations cover realistic experimental imperfections in preparing the x-polarized initial state.

We note that even having the initial state polarized in the z direction will give rise to the same dynamical critical point, but a different order parameter will be required (see Ref. [S7] for details).

To show (i) and (ii), we generalize Eq. (S8) to consider an arbitrary product initial state,

$$|\psi_{\rm in}\left(\boldsymbol{\beta},\boldsymbol{\theta}\right)\rangle=\prod_{i=1}^{L}\left(\sin\beta_i+\cos\beta_i e^{i\Theta_i}a_i^\dagger\right)|0\rangle. \tag{S44}$$

The angles $\{\beta_i\}$ and $\{\Theta_i\}$ characterize any arbitrary product state with each spin pointing along some direction of the Bloch sphere. For uniform global rotations, $(\beta_i,\Theta_i)\equiv(\beta,\Theta)$ for all i.

Recall that the analyticity of the correlation function depends on the occupation of the conserved densities in the initial state, $\langle I_q\rangle_{\rm in}$. For a globally rotated state denoted by $|\beta,\Theta\rangle=|\beta,\Theta\rangle_{\eta=1}+|\beta,\Theta\rangle_{\eta=-1}$, it is straightforward to calculate that in the limit $L\gg1$,

$$\langle b_{-q}b_q\rangle_{{\rm in},\eta}=\frac{-i}{4}e^{2i\theta}\left(\sin2\beta\right)^2\sum_{j=1}^{L}\left[\left(-\cos2\beta\right)^{j-1}-\eta\left(-\cos2\beta\right)^{L-j-1}\right]\sin qj, \tag{S45}$$

$$\left\langle b_q^\dagger b_q\right\rangle_{{\rm in},\eta}=\frac{1}{2}\left(\cos\beta\right)^2\left[1-\eta\left(-\cos2\beta\right)^{L-1}\right]+\frac{1}{4}\left(\sin2\beta\right)^2\sum_{j=1}^{L}\left(-\cos2\beta\right)^{j-1}\left[1-\eta\left(-\cos2\beta\right)^{L-2j}\right]\cos qj, \tag{S46}$$

where we note a difference of a factor of 2 compared with the notation in Sec. S.I B, which is due to the normalization of the states of the even and odd parity sectors. Now, it is obvious that for any initial state with all spins in the $x-y$ plane [i.e., $\beta=\pi/4$, corresponding to case (i) above], the nonanalytic behavior survives, since $1-2\langle I_q\rangle_{\rm in}=\frac{2}{\omega_q}\left[J-B\cos q-J\sin^2q\left(1-\cos\Theta\right)\right]$. This form preserves the nature of the nonanalyticity at the critical point and can be verified in a straightforward manner. Away from the $x-y$ plane [i.e., $\beta\to\frac{\pi}{4}+\epsilon$, corresponding to case (ii)], the initial state will induce small corrections to the value of the correlation function but will not remove the nonanalyticity since it does not change the nature of the pole structure of the integrand [see Eq. (6) in the main text].

To consider initial states of type (iii), we assign any local rotations on the initial spin state to a local unitary operator U_0. Note that by definition of a local operator, we assume U_0 is acting on a finite number of spins for a thermodynamic system. Now consider the order parameter introduced in Eq. (3) of the main text and the difference of its value in the x-polarized initial state $|\psi_{\rm in}\rangle$ and the state perturbed by U_0, itself denoted by $|\psi'_{\rm in}\rangle=U_0|\psi_{\rm in}\rangle$:

$$|G(t)-G'(t)|\leq\|[\frac{1}{L}\sum_i\sigma_i^x(t)\sigma_{i+1}^x(t),U_0]\|, \tag{S47}$$

where $G'(t)$ is defined by Eq. (3) upon replacing the initial state $|\psi_{\rm in}\rangle$ by $|\psi'_{\rm in}\rangle$. Using the Lieb-Robinson bound [S8], we can bound the norm of the commutator to a constant of $\mathcal{O}(1/L)$ for $t=\mathcal{O}(L)$, because within the light cone terms in the commutator decay exponentially in the separation between site i and the sites that U_0 is supported on, leading to a convergent sum. As a result, the difference in the order parameter up to $t=\mathcal{O}(L)$ (which is when the dynamical criticality becomes sharp) is vanishing in the thermodynamic limit, making local perturbations on the initial state largely irrelevant.

[S1] P. Sen and B. K. Chakrabarti, Phys. Rev. B **43**, 13559 (1991).

[S2] A. Lakshminarayan and V. Subrahmanyam, Phys. Rev. A **71**, 062334 (2005).

[S3] M. Frigo and S. G. Johnson, Proc. IEEE **93**, 216 (2005), special issue on "Program Generation, Optimization, and Platform Adaptation".

[S4] M. Suzuki, Phys. Lett. A **146**, 319 (1990).

[S5] D. W. Berry, G. Ahokas, R. Cleve, and B. C. Sanders, Com-

mun. Math. Phys. **270**, 359 (2007).
[S6] A. M. Childs, D. Maslov, Y. Nam, N. J. Ross, and Y. Su, arXiv:1711.10980.
[S7] Y. Li, M. Huo, and Z. Song, Phys. Rev. B **80**, 054404 (2009).
[S8] E. H. Lieb and D. W. Robinson, Comm. Math. Phys. **28**, 251 (1972).